RESEARCH ARTICLE

Check for updates

Na₁₀Zn(NO₃)₄(SO₃S)₄: a nonlinear optical crystal combining inorganic π-conjugated and non-π-conjugated heteroanion groups†

Zihao Yu,[a] Qingran Ding,*[a] Yuhang Jiang,[a] Weiqi Huang,[b] Changsheng Yang,[a] Sangen Zhao [ID] [b] and Junhua Luo [ID] *[a,b]

The research on nonlinear optical (NLO) crystals is mainly focused on two relatively separate systems, π-conjugated or non-π-conjugated systems, respectively. In this work, we report a new NLO crystal Na₁₀Zn (NO₃)₄(SO₃S)₄ combining inorganic π-conjugated [NO₃] and non-π-conjugated heteroanion [S₂O₃] groups, which was synthesized by the aqueous solution method. In the structure, the similar coexistence of planar triangular anionic groups (π-conjugated) and heteroanion tetrahedra (non-π-conjugated) is rarely mentioned, which provides a new approach for designing NLO crystals. Notably, this compound exhibits a phase-matching second-harmonic generation (SHG) response 1.2 times that of KH₂PO₄. In addition, birefringence, absorption edge and theoretical calculations are also reported in this article. This work provides a new designing route to expand NLO systems *via* combining planar π-conjugated and non-π-conjugated heteroanion groups.

Introduction

Nonlinear optical (NLO) crystals have emerged as the core materials of all-solid-state lasers and are widely applied in diverse areas such as high-resolution photoelectron spectroscopy, laser communication, laser prototyping and more.[1–5] Over the past few decades, researchers have displayed persistent research interest in exploring ultraviolet (UV) and deep-UV NLO crystals that exhibit excellent comprehensive properties. Generally, these properties including the second-harmonic generation (SHG) effect, birefringence and band gap are closely related to the structure of crystals.[6] Traditionally, inorganic π-conjugated groups, such as $[BO_3]$,[7] $[CO_3]$,[8] and $[NO_3]$,[9] have been the primary sources for designing and synthesizing high-performance NLO crystals. Some examples include borates ($KBe_2BO_3F_2$,[10] $Li_4Sr(BO_3)_2$,[11] and $Sr_2Be_2B_2O_7$[12]), carbonates ($Ca_2Na_3(CO_3)_3F$),[13] and nitrates ($Ba_2NO_3(OH)_3$).[14] These groups possess delocalized π-electron structures, enabling NLO crystals to exhibit strong SHG effects and birefringence.

The inorganic non-π-conjugated groups (such as $[SO_4]$,[15] $[PO_4]$,[16] and $[SiO_4]$[17]) have received limited attention as NLO materials due to their isotropic tetrahedral structure resulting in compounds with relatively weak birefringence and SHG effects. Until 2014, $Ba_3P_3O_{10}Cl$,[3] as a significant example, confirmed the superior UV transparency properties of NLO crystals constructed with non-π-conjugated groups. This discovery has triggered widespread attention and investigation into non-π-conjugated systems. Subsequently, a series of phosphates, including $Ba_5P_6O_{20}$,[18] Cs_2LiPO_4,[19,20] and $Ba_2NaClP_2O_7$,[21] as well as sulphates $NH_4NaLi_2(SO_4)_2$[22] and silicates $Rb_6Si_{10}O_{23}$,[23] have been reported for deep-UV NLO crystals. Furthermore, new crystals with significant potential in the field of nonlinear optics have been successfully developed, such as $K_2Sb(P_2O_7)F$,[24] $LiHgPO_4$,[25] $[Ag(NH_3)_2]_2SO_4$,[26] CeF_2SO_4[27] and $K_2Mn_3(SO_4)_3F_2·4H_2O$.[28] Recently, researchers have proposed design strategies to improve the birefringence and NLO properties of non-π-conjugated systems.[29] One of these strategies involves the partial substitution of anions in tetrahedral units to form heteroanion groups like $BO_xF_{4−x}$ ($x = 1, 2, 3$),[30] $PO_xF_{4−x}$ ($x = 1, 2, 3$),[31] $SO_xF_{4−x}$ ($x = 1, 2, 3$),[32] and $SiO_xF_{6−x}$ ($x = 1, 2, 3, 4, 5$).[33] Indeed, these non-π-conjugated heteroanion groups result in large birefringence and NLO coefficients of compounds like $NH_4B_4O_6F$,[34] $(NH_4)_2PO_3F$,[31,35] $NaNH_4PO_3F·H_2O$,[35,36] $C(NH_2)_3SO_3F$[37] and so on. Recently, several novel compounds with partial sulfur-substituted groups have been discovered, such as Na_3PO_3S,[38] $Na_{10}Cd(NO_3)_4(SO_3S)_4$,[39] $(C(NH_2)_3)SO_3S$,[40] and $[C(NH_2)_3]_2S_2O_8$.[41] These new partially substituted non-π-conjugated groups exhibit

[a] School of Chemistry and Chemical Engineering, Jiangxi Normal University, Nanchang, 330022, China. E-mail: dqr@jxnu.edu.cn, luojunhua@jxnu.edu.cn
[b] State Key Laboratory of Structural Chemistry, Fujian Institute of Research on the Structure of Matter, Chinese Academy of Sciences, Fuzhou, Fujian 350002, China
†Electronic supplementary information (ESI) available: Thermal stability, elemental analysis, crystallographic data (Tables S1–S5), Raman spectrum, crystal photograph, and crystal thickness. CCDC 2293547 for Na₁₀Zn (NO₃)₄(SO₃S)₄ (**1**). For ESI and crystallographic data in CIF or other electronic format see DOI: https://doi.org/10.1039/d3qi02107f

This journal is © the Partner Organisations 2024

Inorg. Chem. Front., 2024, **11**, 107–113 | **107**

enhanced microscopic properties compared to normal oxygen tetrahedral units (MO_4, where M = B, P, S, Si, *etc.*).

Therefore, both π-conjugated and non-π-conjugated groups have their own structural advantages and have the potential to construct NLO crystals with excellent performance. However, inorganic π-conjugated and non-π-conjugated systems were considered as two relatively separate research subjects in previous studies. The research on NLO crystals combining both inorganic π-conjugated and non-π-conjugated groups has been relatively limited. Recently, Chen's team proposed the π-conjugated confinement principle, which states that separating the non-π-conjugated $[PO_4]$ groups successfully decreases the π-conjugation interaction between $[CO_3]$ units, thereby establishing a connection between π-conjugated and non-π-conjugated groups. Under this guidance, we propose a rational design strategy that combines π-conjugated and non-π conjugated groups to obtain NLO crystals. Thus, we successfully synthesized $Na_{10}Zn(NO_3)_4(SO_3S)_4$ (**1**) which combining the π-conjugated $[NO_3]$ and non-π-conjugated heteroanion $[SO_3S]$ groups. It exhibits a significant SHG effect 1.2 times that of KDP and a short UV absorption edge of 240 nm. The synthesis, elemental analysis, crystal structure, optical properties and theoretical calculations of this compound are also reported in this work.

Experimental section

Reagents and synthesis

All the reagents including $Na_2S_2O_3$ (Tansoole, 99.0%) and $Zn(NO_3)_2 \cdot 6H_2O$ (Aladdin, 99.0%) are of analytical grade obtained from commercial sources without further purification. In this experiment, we obtained the crystals of **1** by a facile aqueous solution method. A mixture of $Na_2S_2O_3$ (0.632 g, 4 mmol) and $Zn(NO_3)_2 \cdot 6H_2O$ (0.297 g, 1 mmol) was dissolved in 10 ml deionized water, and this solution needed heating and stirring for about 30 min until it became clear. Then this solution was allowed to evaporate slowly at room temperature. After several days, colourless single crystals of **1** were obtained.

Single crystal X-ray diffraction

A transparent crystal of compound **1**, measuring 0.08 × 0.03 × 0.03 mm^3, was carefully chosen under an optical microscope for single-crystal X-ray diffraction (XRD) analysis. The diffraction data were acquired at a temperature of 293(2) K using graphite-monochromatized Cu Kα radiation ($\lambda = 1.54178$ Å) on a Rigaku XtaLAB Synergy diffractometer equipped with a HyPix detector. The crystal structure of **1** was successfully determined using the OLEX2 [42] program. The comprehensive details regarding the crystallographic data and the results of the structural refinement for compound **1** can be found in Table S1.† In addition, Tables S2–S5† present the atomic coordinates and corresponding equivalent isotropic displacement parameters, selected bond lengths and angles, as well as the anisotropic displacement parameters (Å^2 × 10^3) for compound **1**.

Powder X-ray diffraction

Powder X-ray diffraction (PXRD) measurements were performed for pure materials using a Miniflex600 powder X-ray diffractometer equipped with Cu Kα radiation ($\lambda = 1.5418$ Å). The diffraction angle was scanned within the range of 5° to 75° with a step width of 0.02°. As depicted in Fig. 1, the experimental X-ray powder patterns of **1** exhibit a high degree of agreement with the values simulated from single-crystal XRD analysis, confirming the purity of **1**.

Elemental analysis

For the elemental analysis of compound **1**, a semiquantitative microprobe was employed in conjunction with a field emission scanning electron microscope (FESEM, SU-80100) that was equipped with an energy dispersive X-ray spectroscope. The energy dispersive spectra were obtained by carefully selecting clean surfaces of the sample for measurement. The presence of Na, Zn, N, O, and S elements of compound **1** was effectively confirmed by energy dispersive X-ray spectra (EDS), as depicted in Fig. S1.† Furthermore, the EDS mapping presented in Fig. 2 illustrates the spatial distribution of these elements.
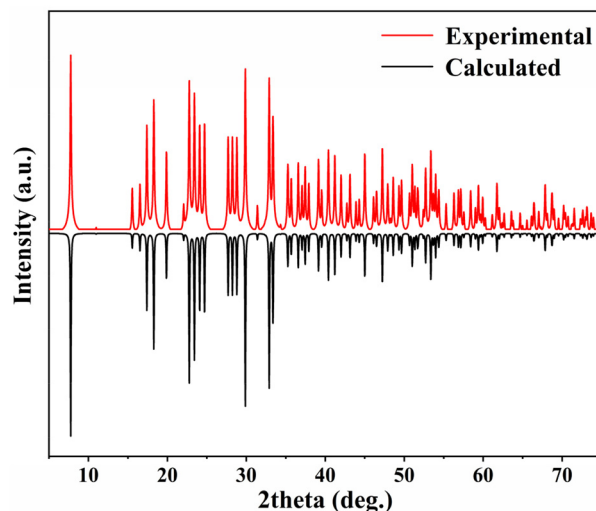

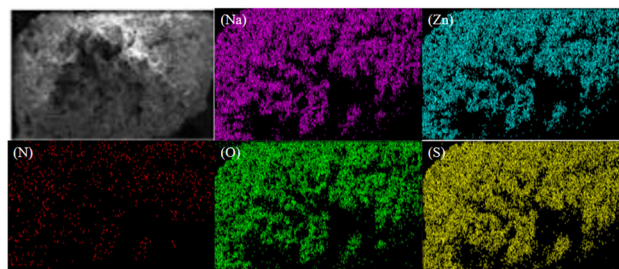**Fig. 1** Experimental and calculated XRD patterns of **1**.

Fig. 2 EDS mapping of sodium (purple), zinc (blue), nitrogen (red), oxygen (green) and sulfur (yellow) on the **1** crystal (top left). The scale bar is 100 μm.

108 | *Inorg. Chem. Front.*, 2024, **11**, 107–113

This journal is © the Partner Organisations 2024

UV-vis-NIR diffuse reflectance spectroscopy

A PerkinElmer Lambda-950 UV/vis/NIR spectrophotometer was used to obtain UV-vis-near-infrared (NIR) diffuse reflection data. The measurements were performed at room temperature within a scan range of 200–800 nm. During the measurement process, $BaSO_4$ powder was used as the standard with 100% reflectance. The recorded data provide information on the diffuse reflection properties of the sample across the specified wavelength range.

SHG measurements

The investigation of the polycrystalline SHG signals of sample **1** was performed using the Kurtz–Perry method.[43] Measurements were conducted using a Q-switched Nd:YAG solid-state laser with a fundamental wavelength of 1064 nm. The crystals **1** were ground and screened into different particle size ranges, namely 45–53 μm, 53–75 μm, 75–105 μm, 105–150 μm, 150–210 μm, and 210–300 μm. Similarly, KH_2PO_4 (KDP) crystals were also processed following the same procedures as that for a reference material. Subsequently, both the samples were placed inside a black box and exposed to pulsed laser irradiation with a wavelength of 1064 nm, allowing further analysis.

Birefringence measurements

To measure the birefringence of the crystal, the interference colour method was employed using a polarizing microscope (ZEISS Axio Scope.A1) equipped with a Berek compensator at a wavelength of 550 nm. The birefringence index (Δn) was calculated using the formula $R = \Delta n \times d$, where R represents the optical path difference obtained using the polarizing microscope, and d represents the crystal thickness measured using the same microscope.

Theoretical calculations

Theoretical calculations based on density functional theory (DFT)[44,45] were performed using the CASTEP package. The exchange–correlation energy was described using the functional developed by Perdew–Burke–Ernzerhof within the generalized gradient approximation (GGA) form. A plane wave cut-off energy of 800 eV was set as the basic cut-off energy. For the numerical integration of the Brillouin zone, the Monkhorst–Pack scheme with a grid density of $3 \times 3 \times 1$ at the k-point was employed for sample **1**.

Results and discussion

Crystal structure

Compound **1** crystallizes in a non-centrosymmetric tetragonal space group of $P\bar{4}$ (no. 81) with unit cell parameters of a = 11.279(2), b = 11.279(2), c = 5.392(2) Å, $\alpha = \beta = \gamma = 90°$, and Z = 1. The unit cell contains one Zn atom, one N atom, two S atoms, three Na atoms and six O atoms. As shown in Fig. 3a, each N atom coordinates with three O atoms to form a π-conjugated [NO_3] group. The distance of the N–O bond
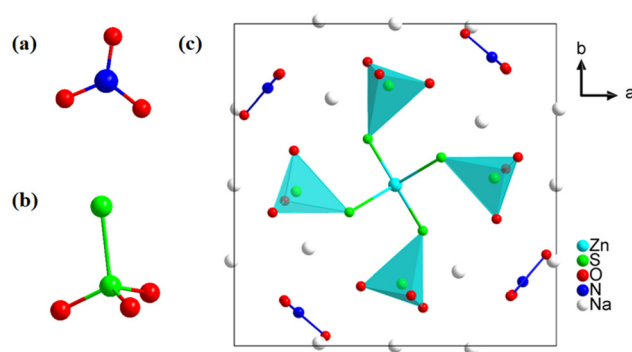

Fig. 3 (a) π-Conjugated [NO_3] group. (b) Non-π-conjugated heteroanion [SO_3S] group; (c) the crystal structure of **1** viewed along the c axis.

ranges from 1.248(3) to 1.253(3) Å. Two sulfur atoms are present in different oxidation states: −2 and +6, respectively. Each S^{6+} atom, serving as the central atom in a tetrahedron, coordinates with three oxygen atoms and one S^{2-} atom to form a non-π-conjugated heteroanion [SO_3S] group (Fig. 3b). Meanwhile, the S^{2-} atom forms an S=S double bond with a bond length of 2.027(7) Å. Based on the $\bar{4}$ symmetry operation, four heteroanion [SO_3S] groups further connect with the central Zn atom which is located at the face-centered (the center of the ab plane) position of the unit cell through their S^{2-} atoms, forming an isolated $Zn(SO_3S)_4$ moiety (Fig. 3c). The π-conjugated [NO_3] groups dispersed between each [SO_3S] moiety through four-fold rotational reflection symmetry operations. Meanwhile, the Na^+ cation serves as a charge-balancing cation filled in gaps. To further identify the S=S bond in **1**, the Raman spectrum is shown in Fig. S2.† The peak at 476 cm^{-1} presents the symmetrical stretching mode of the S=S bond.[46] In addition, for the growth of large-sized single crystals, we made preliminary attempts and provided a photograph of the crystal (refer to Fig. S3†).

UV-vis-NIR diffuse reflectance spectra

As illustrated in Fig. 4, the UV-vis-NIR diffuse reflection spectrum of **1** shows that its reflectance is about 10% at a wavelength of 240 nm. Based on Kubelka–Munk function,[47] the reflectance can be used to calculate the experimental energy gap. By applying this approach, the experimental energy gap of **1** was deduced to be 4.02 eV, thus indicating its potential applications in the UV spectral range.

NLO properties

The powder SHG response of crystal **1** was measured under 1064 nm laser irradiation using the Kurtz–Perry method,[48] and KDP crystals used as a reference. As indicated in Fig. 5a, the SHG intensity will increase simultaneously with the increasing particle size until it reaches a stable value, which suggests that compound **1** is phase matchable. Specifically, with the particle size of the powder in the range of 210–300 μm, the intensity of the SHG signal for compound **1** is approximately 1.2 times that of the KDP (Fig. 5b). The SHG effect of **1** was superior to
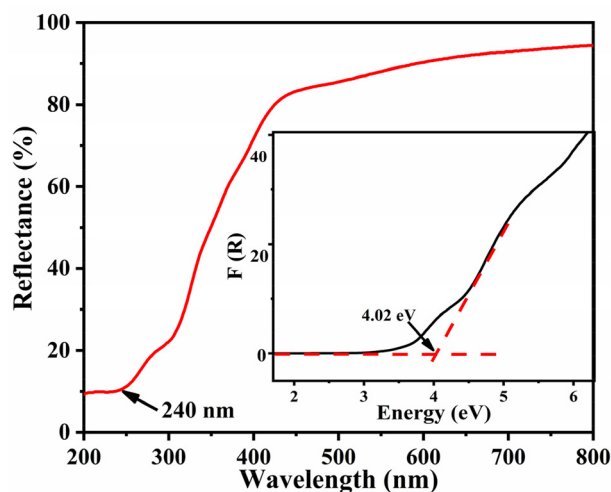
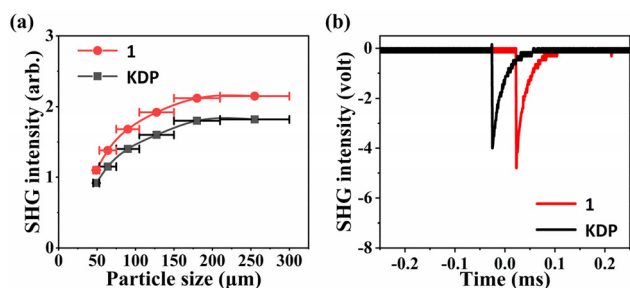Fig. 4 UV-visible-NIR diffuse reflectance spectrum of **1**.

Fig. 6 (a) Single crystal of **1** under the polarizing microscope. (b) Crystal achieves complete extinction under the Beret compensator.

Fig. 5 (a) SHG intensity *vs.* particle sizes at λ = 1064 nm for **1**. (b) SHG signals of **1** as compared with the KDP reference.

Fig. 7 Calculated refractive index and birefringence of **1**.

those of some sulphates such as $Cs_2Zn_2(SO_4)_3$ (0.15 × KDP),[15] $Cs_2Ca_2(SO_4)_3$ (0.6 × KDP),[49] $K_2Zn_3(SO_4)(HSO_4)_2F_4$ (0.3 × KDP),[50] $(NH_4)_2Na_3Li_9(SO_4)_7$ (0.5 × KDP),[22] $KTb(SO_4)_2$ (0.3 × KDP),[51] and $Li_8NaRb_3(SO_4)_6 \cdot 2H_2O$ (0.3 × KDP).[52] In addition, compared to other NLO materials containing inorganic π-conjugated and non-π-conjugated groups, compound **1** exhibits comparable or even better SHG effects. Examples of such compounds include $Ba_4(BO_3)_3(SiO_4)Cl \cdot Ba_3X$ (X = Cl, Br) (1 × KDP),[17] $Ba_3Ca_4(BO_3)_3(SiO_4)Cl$ (0.6 × KDP),[53] $(NH_4)_2B_4SO_{10}$ (1.1 × KDP)[54] and so on. Therefore, we can draw a conclusion that compound **1** exhibits a significant SHG effect. It is worth noting that such NLO crystals combining inorganic π-conjugated and non-π-conjugated groups are still in their infancy; there is much unexplored space, indicating the need for further research in this field.

Birefringence

The experimental birefringence of crystal **1** was determined by the method of detecting interference colours under a polarizing microscope. It was observed that crystal **1** exhibited interference effects under linearly polarized light (refer to Fig. 6a). Subsequently, by inserting a compensator and adjusting appropriately, complete compensation of the phase difference
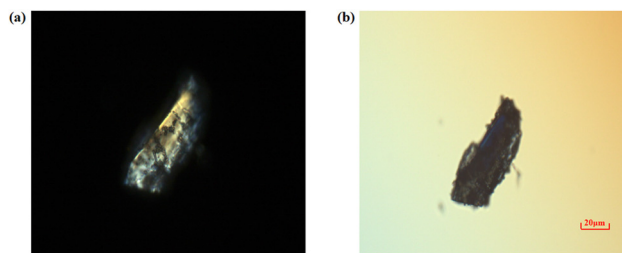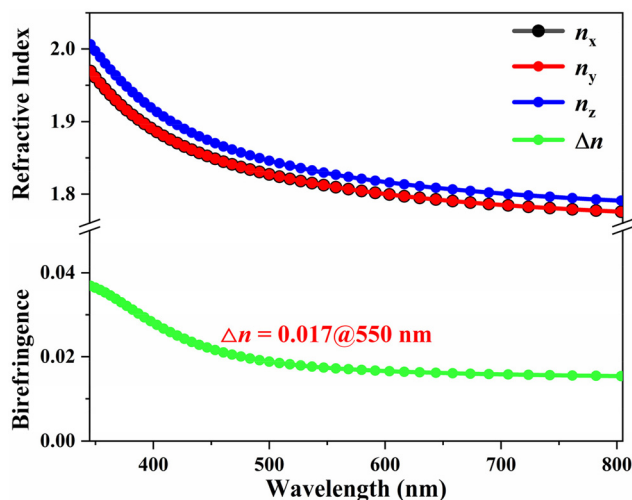
of light is achieved, resulting in the complete extinction of interference effects. In this case, crystal **1** achieved complete extinction, appearing black, which indicates its birefringent properties. Additionally, the optical path difference of the crystal was 306.3 nm according to the reading of the compensator. Using the polarizing microscope, further measurements determined that the thickness of crystal **1** is 23.02 μm (Fig. S5†). By plugging the above numerical value into the formula, the birefringence of crystal **1** is determined to be approximately 0.013 at a wavelength of 550 nm.

In addition, the birefringence of crystal **1** at a wavelength of 550 nm, calculated using the first-principles method, is determined to be 0.017 (see Fig. 7). The consistency between the theoretical value and the experimental measurement indicates that the birefringence we obtained is reliable.

Theoretical calculations

To further gain a comprehensive understanding of the relationship between the structures and properties, we carried out theoretical calculations based on density functional theory. The electronic band structure analysis suggests that **1** has an indirect band gap of 2.59 eV (Fig. 8a), which is consistent with the experimental result based on the single crystal
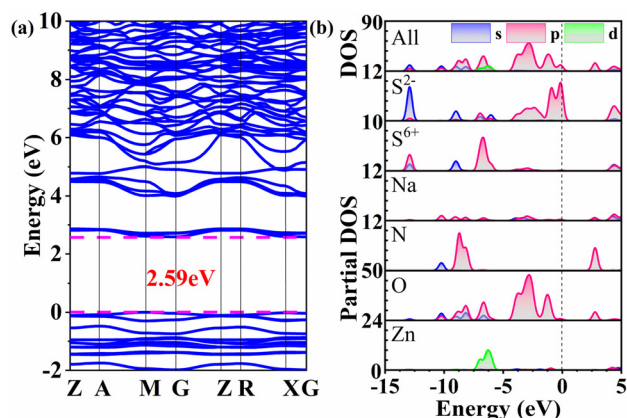
Fig. 8 (a) Electronic band structure of **1**. (b) DOS and partial DOS of **1**.

sample. In the investigation of the optical properties of materials, the focus is on analysing electron transitions that occur between the top of the valence band and the bottom of the conduction band. Therefore, Fig. 8b depicts the total density of states (DOS) and the partial DOS of **1**, providing a visual representation of the distribution of electronic states for that specific element. At the top of the valence band, ranging from −5 to 0 eV, it is primarily occupied by S 3p (especially for S^{2-}) and O 2p orbitals, where the S 3p orbitals originate from the non-π-conjugated [SO_3S] groups. Conversely, the bottom of the conduction band is predominantly composed of N 2p and O 2p orbitals, where the N 2p orbitals originate from the π-conjugated [NO_3] groups. It can be concluded that these optical properties of **1** are mainly determined by the π-conjugated [NO_3] groups and the non-π-conjugated heteroanionic [SO_3S] groups, and the contribution of Na and Zn cations can be neglected. It is necessary to point out that combining non-π-conjugated heteroanionic groups with π-conjugated groups is an effective strategy for obtaining compounds with excellent optical properties and its potential needs further exploration.

Conclusions

In conclusion, we successfully synthesized a NLO crystal $Na_{10}Zn(NO_3)_4(SO_3S)_4$ *via* a facile water solution method. The single crystal structure analysis confirmed the presence of π-conjugated [NO_3] groups and non-π-conjugated [SO_3S] groups in this material, as further confirmed through EDS and Raman measurements. Experimental and calculation results demonstrate its excellent optical properties, including diffuse reflectance, SHG and birefringence. It is particularly noteworthy that this compound exhibits a significant SHG response, 1.2 times that of KDP. Theoretical calculations indicate that the synergistic interaction between the π-conjugated [NO_3] groups and the non-π-conjugated heteroanionic [SO_3S] groups makes the primary contribution. This finding provides new possibilities for designing novel NLO materials by com-

bining different conjugated groups such as π-conjugated and non-π-conjugated heteroanionic groups.

Author contributions

Junhua Luo provided research ideas and supervised the entire research. Sangen Zhao was responsible for theoretical calculations. Zihao Yu completed the entire experimental work. Yuhang Jiang and Weiqi Huang assisted in the experiments. Changsheng Yang assisted in the PXRD measurements. Qingran Ding wrote the initial draft and revised the manuscript. All authors participated in the discussion.

Conflicts of interest

There are no conflicts to declare.

Acknowledgements

Notes and references

1 D. F. Eaton, Nonlinear optical materials, *Science*, 1991, **253**, 281–287.

2 D. Cyranoski, China's crystal cache: a Chinese laboratory is the only source of a valuable crystal. David Cyranoski investigates why it won't share its supplies, *Nature*, 2009, **457**, 953–956.

3 P. Yu, L. M. Wu, L. J. Zhou and L. Chen, Deep-Ultraviolet Nonlinear Optical Crystals: $Ba_3P_3O_{10}X$ (X = Cl, Br), *J. Am. Chem. Soc.*, 2014, **136**, 480–487.

4 Y. N. Xia, C. T. Chen, D. Y. Tang and B. C. Wu, New nonlinear optical crystals for UV and VUV harmonic generation, *Adv. Mater.*, 1995, **7**, 79–81.

5 H. W. Huang, L. J. Liu, S. F. Jin, W. J. Yao, Y. H. Zhang and C. T. Chen, Deep-Ultraviolet Nonlinear Optical Materials: $Na_2Be_4B_4O_{11}$ and $LiNa_5Be_{12}B_{12}O_{33}$, *J. Am. Chem. Soc.*, 2013, **135**, 18319–18322.

6 J. Chen, Q. Q. Chen, F. F. Mao, Z. Liu, B. X. Li, X. H. Wu and K. Z. Du, $Ba_4Ag_5(IO_3)_6(I_3O_8)_3(I_4O_{11})_2$:A Nonlinear

This journal is © the Partner Organisations 2024

Inorg. Chem. Front., 2024, **11**, 107–113 | **111**

Optical Crystal Containing Two Types of Polyiodate Anions, *Inorg. Chem. Front.*, 2022, **9**, 5917–5925.

7 M. Mutailipu, M. Zhang, H. P. Wu, Z. H. Yang, Y. H. Shen, J. L. Sun and S. L. Pan, $Ba_3Mg_3(BO_3)_3F_3$ polymorphs with reversible phase transition and high performances as ultraviolet nonlinear optical materials, *Nat. Commun.*, 2018, **9**, 3089.

8 X. M. Liu, L. Kang, P. F. Gong and Z. S. Lin, $LiZn(OH)CO_3$: A Deep-Ultraviolet Nonlinear Optical Hydroxycarbonate Designed from a Diamond-like Structure, *Angew. Chem., Int. Ed.*, 2021, **60**, 13574–13578.

9 S. G. Zhao, Y. Yang, Y. G. Shen, B. Q. Zhao, L. N. Li, C. M. Ji, Z. Y. Wu, D. Q. Yuan, Z. S. Lin, M. C. Hong and J. H. Luo, Cooperation of Three Chromophores Generates the Water-Resistant Nitrate Nonlinear Optical Material $Bi_3TeO_6OH(NO_3)_2$, *Angew. Chem., Int. Ed.*, 2017, **56**, 540–544.

10 B. C. Wu, D. Y. Tang, N. Ye and C. T. Chen, Linear and nonlinear optical properties of the $KBe_2BO_3F_2$ (KBBF) crystal, *Opt. Mater.*, 1996, **5**, 105–109.

11 S. G. Zhao, P. F. Gong, L. Bai, X. Xu, S. Q. Zhang, Z. H. Sun, Z. S. Lin, M. C. Hong, C. T. Chen and J. H. Luo, Beryllium-free $Li_4Sr(BO_3)_2$ for deep-ultraviolet nonlinear optical applications, *Nat. Commun.*, 2014, **5**, 4019.

12 C. T. Chen, Y. B. Wang, B. C. Wu, K. C. Wu, W. L. Zeng and L. H. Yu, Design and synthesis of an ultraviolet-transparent nonlinear optical crystal $Sr_2Be_2B_2O_7$, *Nature*, 1995, **373**, 322–324.

13 M. Luo, Y. X. Song, C. S. Lin, N. Ye, W. D. Cheng and X. F. Long, Molecular Engineering as an Approach To Design a New Beryllium-Free Fluoride Carbonate as a Deep-Ultraviolet Nonlinear Optical Material, *Chem. Mater.*, 2016, **28**, 2301–2307.

14 X. H. Dong, L. Huang, Q. Y. Liu, H. M. Zeng, Z. E. Lin, D. G. Xu and G. H. Zou, Perfect balance harmony in $Ba_2NO_3(OH)_3$: a beryllium-free nitrate as a UV nonlinear optical material, *Chem. Commun.*, 2018, **54**, 5792–5795.

15 Y. C. Liu, Y. Q. Li, Y. Zhou, Q. R. Ding, Y. X. Chen, S. G. Zhao and J. H. Luo, A new nonlinear optical sulfate of layered structure: $Cs_2Zn_2(SO_4)_3$, *Inorg. Chem. Commun.*, 2021, **124**, 108390.

16 L. Xiong, L. M. Wu and L. Chen, A General Principle for DUV NLO Materials: π-Conjugated Confinement Enlarges Band Gap, *Angew. Chem., Int. Ed.*, 2021, **60**, 25063–25067.

17 X. X. Lin, F. F. Zhang, S. L. Pan, H. W. Yu, F. Y. Zhang, X. Y. Dong, S. J. Han, L. Y. Dong, C. Y. Bai and Z. Wang, $Ba_4(BO_3)_3(SiO_4)·Ba_3X$ (X = Cl, Br): new salt-inclusion borosilicate halides as potential deep UV nonlinear optical materials, *J. Mater. Chem. C*, 2014, **2**, 4257–4264.

18 S. G. Zhao, P. F. Gong, S. Y. Luo, L. Bai, Z. S. Lin, Y. Y. Tang, Y. L. Zhou, M. C. Hong and J. H. Luo, Tailored Synthesis of a Nonlinear Optical Phosphate with a Short Absorption Edge, *Angew. Chem., Int. Ed.*, 2015, **54**, 4217–4221.

19 Y. G. Shen, Y. Yang, S. G. Zhao, B. Q. Zhao, Z. S. Lin, C. M. Ji, L. N. Li, P. Fu, M. C. Hong and J. H. Luo, Deep-

Ultraviolet Transparent Cs_2LiPO_4 Exhibits an Unprecedented Second Harmonic Generation, *Chem. Mater.*, 2016, **28**, 7110–7116.

20 L. Li, Y. Wang, B. H. Lei, S. J. Han, Z. H. Yang, K. R. Poeppelmeier and S. L. Pan, A New Deep-Ultraviolet Transparent Orthophosphate $LiCs_2PO_4$ with Large Second Harmonic Generation Response, *J. Am. Chem. Soc.*, 2016, **138**, 9101–9104.

21 J. Chen, L. Xiong, L. Chen and L. M. Wu, $Ba_2NaClP_2O_7$: Unprecedented Phase Matchability Induced by Symmetry Breaking and Its Unique Fresnoite-Type Structure, *J. Am. Chem. Soc.*, 2018, **140**, 14082–14086.

22 Y. Q. Li, F. Liang, S. G. Zhao, L. N. Li, Z. Y. Wu, Q. R. Ding, S. Liu, Z. S. Lin, M. C. Hong and J. H. Luo, Two Non-π-Conjugated Deep-UV Nonlinear Optical Sulfates, *J. Am. Chem. Soc.*, 2019, **141**, 3833–3837.

23 S. Z. Huang, Y. Yang, J. B. Chen, W. Q. Jin, S. C. Cheng, Z. H. Yang and S. L. Pan, "Removing Center"—An Effective Structure Design Strategy for Nonlinear Optical Crystals, *Chem. Mater.*, 2022, **34**, 2429–2438.

24 Y. L. Deng, L. Huang, X. H. Dong, L. Wang, K. M. Ok, H. M. Zeng, Z. E. Lin and G. H. Zou, $K_2Sb(P_2O_7)F$: Cairo Pentagonal Layer with Bifunctional Genes Reveal Optical Performance, *Angew. Chem., Int. Ed.*, 2020, **59**, 21151–21156.

25 B. L. Wu, C. L. Hu, F. F. Mao, R. L. Tang and J. G. Mao, Highly Polarizable Hg^{2+} Induced a Strong Second Harmonic Generation Signal and Large Birefringence in $LiHgPO_4$, *J. Am. Chem. Soc.*, 2019, **141**, 10188–10192.

26 Y. C. Yang, X. Liu, J. Lu, L. M. Wu and L. Chen, $[Ag(NH_3)_2]_2SO_4$: A Strategy for the Coordination of Cationic Moieties to Design Nonlinear Optical Materials, *Angew. Chem., Int. Ed.*, 2021, **60**, 21216–21220.

27 C. Wu, T. H. Wu, X. X. Jiang, Z. J. Wang, H. Y. Sha, L. Lin, Z. S. Lin, Z. P. Huang, X. F. Long, M. G. Humphrey and C. Zhang, Large Second-Harmonic Response and Giant Birefringence of $CeF_2(SO_4)$ Induced by Highly Polarizable Polyhedra, *J. Am. Chem. Soc.*, 2021, **143**, 4138–4142.

28 Y. Zhou, Y. Q. Li, Q. R. Ding, Y. C. Liu, Y. X. Chen, X. T. Liu, X. Y. Huang, L. N. Li, S. G. Zhao and J. H. Luo, Noncentrosymmetric $K_2Mn_3(SO_4)_3F_2·4H_2O$ and $Rb_2Mn_3(SO_4)_3F_2·2H_2O$ with pseudo-KTP structures, *Chin. Chem. Lett.*, 2021, **32**, 263–265.

29 H. Y. Wu, C. L. Hu, M. B. Xu, Q. Q. Chen, N. Ma, X. Y. Huang, K. Z. Du and J. Chen, From $H_{12}C_3N_2CdI_4$ to $H_{11}C_4N_2CdI_3$: a highly polarizable $CdNI_3$ tetrahedron induced a sharp enhancement of second harmonic generation response and birefringence, *Chem. Sci.*, 2023, **14**, 9533–9542.

30 B. B. Zhang, G. Q. Shi, Z. H. Yang, F. F. Zhang and S. L. Pan, Fluorooxoborates: Beryllium-Free Deep-Ultraviolet Nonlinear Optical Materials without Layered Growth, *Angew. Chem., Int. Ed.*, 2017, **56**, 3916–3919.

31 B. B. Zhang, G. P. Han, Y. Wang, X. L. Chen, Z. H. Yang and S. L. Pan, Expanding Frontiers of Ultraviolet Nonlinear

Optical Materials with Fluorophosphates, *Chem. Mater.*, 2018, **30**, 5397–5403.

32 W. Q. Jin, W. Y. Zhang, A. Tudi, L. Y. Wang, X. Zhou, Z. H. Yang and S. L. Pan, Fluorine-Driven Enhancement of Birefringence in the Fluorooxosulfate: A Deep Evaluation from a Joint Experimental and Computational Study, *Adv. Sci.*, 2021, **8**, 2003594.

33 Q. R. Ding, X. M. Liu, S. G. Zhao, Y. S. Wang, Y. Q. Li, L. N. Li, S. Liu, Z. S. Lin, M. C. Hong and J. H. Luo, Designing a Deep-UV Nonlinear Optical Fluorooxosilicophosphate, *J. Am. Chem. Soc.*, 2020, **142**, 6472–6476.

34 G. Q. Shi, Y. Wang, F. F. Zhang, B. B. Zhang, Z. H. Yang, X. L. Hou, S. L. Pan and K. R. Poeppelmeier, Finding the Next Deep-Ultraviolet Nonlinear Optical Material: $NH_4B_4O_6F$, *J. Am. Chem. Soc.*, 2017, **139**, 10645–10648.

35 L. Xiong, J. Chen, J. Lu, C. Y. Pan and L. M. Wu, Monofluorophosphates: A New Source of Deep-Ultraviolet Nonlinear Optical Materials, *Chem. Mater.*, 2018, **30**, 7823–7830.

36 J. Lu, J. N. Yue, L. Xiong, W. K. Zhang, L. Chen and L. M. Wu, Uniform Alignment of Non-π-Conjugated Species Enhances Deep Ultraviolet Optical Nonlinearity, *J. Am. Chem. Soc.*, 2019, **141**, 8093–8097.

37 M. Luo, C. S. Lin, D. H. Lin and N. Ye, Rational Design of the Metal-Free $KBe_2BO_3F_2$·(KBBF) Family Member $C(NH_2)_3SO_3F$ with Ultraviolet Optical Nonlinearity, *Angew. Chem., Int. Ed.*, 2020, **59**, 15978–15981.

38 X. Y. Zhang, L. Kang, P. F. Gong, Z. S. Lin and Y. C. Wu, Nonlinear Optical Oxythiophosphate Approaching the Good Balance with Wide Ultraviolet Transparency, Strong Second Harmonic Effect, and Large Birefringence, *Angew. Chem., Int. Ed.*, 2021, **60**, 6386–6390.

39 Y. C. Liu, Y. Q. Liu, Z. S. Lin, Y. Q. Li, Q. R. Ding, X. Chen, L. N. Li, S. G. Zhao, M. C. Hong and J. H. Luo, Nonpolar $Na_{10}Cd(NO_3)_4(SO_3S)_4$ Exhibits a Large Second-Harmonic Generation, *CCS Chem.*, 2022, **4**, 526–531.

40 Y. C. Liu, X. M. Liu, Z. Y. Xiong, B. W. Liu, J. L. Xu, L. N. Li, S. G. Zhao, Z. S. Lin, M. C. Hong and J. H. Luo, 2D van der Waals Layered $[C(NH_2)_3]_2SO_3S$ Exhibits Desirable UV Nonlinear-Optical Trade-Off, *Inorg. Chem.*, 2021, **60**, 14544–14549.

41 M. Zhang, B. B. Zhang, D. Q. Yang and Y. Wang, $[C(NH_2)_3]_2S_2O_8$: combining delocalized and localized π-conjugate units to achieve strong optical anisotropy, *Inorg. Chem. Front.*, 2022, **9**, 6067–6074.

42 O. V. Dolomanov, L. J. Bourhis, R. J. Gildea, J. A. K. Howard and H. Puschmann, OLEX2: a complete structure solution, refinement and analysis program, *J. Appl. Crystallogr.*, 2009, **42**, 339–341.

43 S. K. Kurtz and T. T. Perry, A Powder Technique for the Evaluation of Nonlinear Optical Materials, *J. Appl. Phys.*, 1968, **39**, 3798–3813.

44 W. Kohn, Nobel Lecture: Electronic structure of matter—wave functions and density functionals, *Rev. Mod. Phys.*, 1999, **71**, 1253–1266.

45 S. J. Clark, M. D. Segall, C. J. Pickard, P. J. Hasnip, M. I. J. Probert, K. Refson and M. C. Payne, First principles methods using CASTEP, *Z. Kristallogr. - Cryst. Mater.*, 2005, **220**, 567–570.

46 J. Z. Zhou, Y. Chu, J. J. Li and S. L. Pan, Ba_2BS_3Cl and $Ba_5B_2S_8Cl_2$: first alkaline-earth metal thioborate halides with $[BS_3]$ units, *Chem. Commun.*, 2021, **57**, 6440–6443.

47 P. Kubelka and F. Munk, An article on optics of paint layers, *Z. Tech. Phys.*, 1931, **12**, 259–274.

48 M. R. Sun, G. L. Wang and J. Y. Yao, The Kurtz–Perry Powder Technique Revisited: A Study of the Effect of Reference Selection on Powder Second-Harmonic Generation Response, *Molecules*, 2023, **28**, 1116.

49 Y. G. Shen, X. L. Xue, W. Y. Tu, Z. Q. Liu, R. W. Yan, H. Zhang and J. R. Jia, Synthesis, Crystal Structure, and Characterization of a Noncentrosymmetric Sulfate $Cs_2Ca_2(SO_4)_3$, *Eur. J. Inorg. Chem.*, 2020, 854–858.

50 Y. Zhou, X. Y. Zhang, Z. Y. Xiong, X. F. Long, Y. Q. Li, Y. X. Chen, X. Chen, S. G. Zhao, Z. S. Lin and J. H. Luo, Non-π-Conjugated Deep-Ultraviolet Nonlinear Optical Crystal $K_2Zn_3(SO_4)(HSO_4)_2F_4$, *J. Phys. Chem. Lett.*, 2021, **12**, 8280–8284.

51 Q. Wu, C. Yang, J. Ma, F. Liang, C. L. Teng and Y. S. Du, Synthesis, Crystal Structure, and Nonlinear Optical Property of an Anhydrous Sulfate $KTb(SO_4)_2$, *Inorg. Chem.*, 2021, **60**, 15041–15047.

52 Y. Q. Li, S. G. Zhao, P. Shan, X. F. Li, Q. R. Ding, S. Liu, Z. Y. Wu, S. S. Wang, L. N. Li and J. H. Luo, $Li_8NaRb_3(SO_4)_6·2H_2O$ as a new sulfate deep-ultraviolet nonlinear optical material, *J. Mater. Chem. C*, 2018, **6**, 12240–12244.

53 Z. X. Lu, F. F. Zhang, A. Tudi, S. J. Yu, Z. H. Yang and S. L. Pan, $Ba_3Ca_4(BO_3)_3(SiO_4)Cl$: a new non-centro-symmetric complex alkaline-earth metal borosilicate chloride with a deep-ultraviolet cut-off edge, *Inorg. Chem. Front.*, 2019, **6**, 2200–2208.

54 Z. J. Li, W. Q. Jin, F. F. Zhang, Z. L. Chen, Z. H. Yang and S. L. Pan, Achieving Short-Wavelength Phase-Matching Second Harmonic Generation in Boron-Rich Borosulfate with Planar $[BO_3]$ Units, *Angew. Chem., Int. Ed.*, 2022, **61**, e202112844.

This journal is © the Partner Organisations 2024

Inorg. Chem. Front., 2024, **11**, 107–113 | **113**